Journal of Materials Chemistry A

Transition Metal Inverse-Hybrid Perovskites

Journal:	*Journal of Materials Chemistry A*
Manuscript ID	TA-COM-03-2018-002785.R1
Article Type:	Communication
Date Submitted by the Author:	21-Jun-2018
Complete List of Authors:	Gebhardt, Julian; University of Pennsylvania School of Arts and Sciences, Chemistry Rappe, Andrew; University of Pennsylvania, Department of Chemistry

Journal Name

ARTICLE TYPE

Cite this: DOI: 10.1039/xxxxxxxxxx

Transition Metal Inverse-Hybrid Perovskites†

Julian Gebhardt*[ab‡] and Andrew M. Rappe[a]

Received Date
Accepted Date

DOI: 10.1039/xxxxxxxxxx

www.rsc.org/journalname

Inverse-hybrid perovskites are related to the photovoltaically promising hybrid perovskites by inverting ion positions. While research of this young materials class focused on main-group elements, here we present an investigation of transition metals (TMs) as mono- or divalent anions in methyl ammonium $(MA)_3BA$ compounds. We find that TMs are best employed on the A-site. First, this allows for favorable tolerance factors in $(MA)_3FA$ compounds and second, most B-site TMs form covalent bonds with neighboring hydrogen atoms or A-site ions, leading to non-perovskite structures. Among the fluoride compounds, group X TMs Ni and Pd yield band gaps of 1.11 eV to 1.35 eV, respectively, low effective masses, and are predicted to have favorable defect tolerance. Thus, they are perfect candidates for photovoltaic applications and are potential lead-free alternatives to $MAPbI_3$.

1 Introduction

We previously proposed inverse-hybrid perovskites (IHPs) as intriguing new perovskite modification with interesting band topology and potential use in ferroelectric applications.[1,2] Besides investigations on extended metal-organic frameworks with tetrathiafulvalene radicals,[3–5] this was the first time X_3BA compounds in the inverse (or anti) perovskite structure with inverted ionic charge employed an organic ion. Furthermore, compositions with band gaps toward the upper part of the range that is relevant for photovoltaics (PV) were proposed.[6] In our initial report,[1] we found that incorporating transition metals (TM) can reduce the band gap significantly by fractionally filling their valence d states. Thus, in order to broaden the class of lead-free materials[7–9] that could potentially challenge hybrid perovskites for PV applications[10–12] and to deepen our knowledge of IHPs, in this work we systematically consider the inclusion of transition metal (TM) elements as mono- or divalent anions into X_3BA materials with $X = CH_3NH_3^+$ (MA).

2 Computational Details

Structures were fully optimized by non-spin-polarized (unless noted otherwise) density-functional theory (DFT). We use the Perdew–Burke–Ernzerhof (PBE) generalized gradient approximation[13] as implemented in the Quantum Espresso package[14], supplemented by the D2 method[15] in order to account for dispersive interactions. Core electrons are treated by norm–conserving, optimized, nonlocal, scalar-relativistic pseudopotentials generated with Opium[16–18]. In cases where spin-orbit coupling (SOC) plays an important role, a fully-relativistic treatment was employed to investigate the difference on the electronic structure. Wave functions are expanded in a plane–wave basis with an energy cutoff of 680 eV. Total energies and atomic structures are fully relaxed to 10^{-7} eV/cell and until forces acting on ions are below 0.0025 eV/Å. The Brillouin zone is sampled by a 6×6×6 Monkhorst-Pack **k**-point grid[19], whereas a denser grid of 18×18×18 **k** points was used for calculating the density of states (DoS). For details on the structural sampling see our previous works.[1,6] Reference compounds MAa^- and $(MA)_2a^{2-}$ are also described in our previous works. For cases of interest, we compare the PBE with HSE06[20] results for a better quantitative estimate of the band gap. The Fock operator for the HSE06 calculation was represented on a 3×3×3 **q** point grid using a kinetic energy cutoff of 200 Ry and 216 **k** points. The band structure interpolation was performed with Wannier90.[21] Effective masses were obtained as described in[22].

3 Results and Discussion

As a design principle in our materials search,[1,6] we employ tolerance factors t[23] in order to assess the suitability of compositions to crystallize in the perovskite structure. For main group IHPs, we found that a threshold of $t > 0.76$ has to be met, wheras a different phase ($CaIrO_3$) is more stable for smaller t.[6] Deviations from perfect ionic radii ratios for $0.76 < t < 1$ are balanced by tilting of the X-site cations (MA) rather than octahedral rotations. The

[a] Department of Chemistry, University of Pennsylvania, Philadelphia, Pennsylvania 19104-6323, United States, jugeb@sas.upenn.edu
[b] Max Planck Institute for the Structure and Dynamics of Matter, Luruper Chaussee 149, 22761 Hamburg, Germany

† Electronic Supplementary Information (ESI) available: Optimized geometries of table Table 1 as well as of the most stable phase of the reference compounds MAa^- and $(MA)_2a^{2-}$. Discussion of defect tolerance for $(MA)_3FNi$ and $(MA)_3FPd$. See DOI: 10.1039/b000000x/

ionic radii to determine t were taken from the table of Shannon and Prewitt[24,25] whenever possible. However, since the latter is incomplete for anionic species, especially for metals that occur mostly as cations, we recently developed a model that allows to estimate effective ionic radii for elements, oxidation states, and coordination numbers that are not present in previously tabulated data.[26] This methodology is applied here. Note however, that the lower number of known crystals that contain TMs in anionic oxidation states leads to larger uncertainties in the determined effective radii compared to halides or chalcogenides.

3.1 Filled d shell

In our previous works, we found that the valence p shell of metals with large SOC can be employed to open small gaps by fractional filling. Such a gap can either be introduced between the $j = 1/2$ and $j = 3/2$ bands by filling two states, or between the two sets of $j = 3/2$ bands in the case of four filled states. With TMs, divalent group XII elements could be an alternative to monovalent group XIII elements for the first gap type. We test this possibility for the fluoride compounds of Zn^{2-}, Cd^{2-}, and Hg^{2-}. All $(MA)_3FA$ compounds have tolerance factors close to 1, and consequently cubic perovskites are predicted. Electronically, all show a filled TM d shell with TM p bands at the Fermi level (Fig. 1 (a)). For the lighter elements (Zn and Cd), the splitting between the p bands is too small to introduce a band gap at the PBE (Fig. 1 (b,c)) or the HSE level (not shown), analogously to $(MA)_3FPb$. For the element with maximal SOC in this group, Hg (Fig. 1 (d)), this is different. At the more reliable HSE level, the larger SOC splitting between $j = 1/2$ and $j = 3/2$ bands opens a small band gap of 0.19 eV. In addition, the splitting of the three pairs of TM p bands is noticeably reduced with the elemental weight, leading to almost degenerate bands in the case of Zn. The interesting features with linear band dispersion of the valence p bands at high symmetry points are observed for all three compounds.

3.2 Fractionally filled d shell

Next, we move on to using the TM d shell as valence. To do so, we first consider the crystal field splitting for TMs on the A and B site, respectively. While a TM on the B-site should have an octahedral crystal field splitting with t_{2g} below e_g states, within the cuboctahedron on the A-site, a dodecahedral crystal field splitting with reversed band order can be expected (Fig. 2).[27] This means, that a different number of d electrons is required for fractional filling the d states in a way that e_g and t_{2g} states are empty, filled, or half-filled so that a gap can be introduced between them.

On the A-site, elements with d^2, d^3, d^5, and d^8 (d^0 can be neglected since alkaline-earth metals are unable to exist in oxidation states other than +2) filling are expected to yield favorable divalent anions, whereas d^1, d^3, d^4, d^6, and d^8 elements are promising on the B-site. Employing TMs as monovalent ions comes with the same caveat identified for p shell metals:[6] O and S are protonated on the B-site. Therefore, if IHPs without such B-site protonation are desired, suitable divalent partners (chalcogenides) are more scarce compared to monovalent anions (halides). Furthermore, TMs are rather large, favoring a combination with smaller anions.

Nevertheless, TMs with d^1, d^3, d^4, d^6, and d^9 filling should have favorable electron configurations to serve as monovalent anions on the A-site, whereas this is the case for d^2, d^4, d^5, d^7, and d^9 elements for the B-site, and we will assess the possibility for suitable compounds also for these monovalent TMs.

3.3 Divalent anions on the A-site

We start with the most promising group, TMs as large divalent anions on the A-site, paired with a small monovalent B-site anion. According to our considerations above, we first investigate the d^2 metal titanium. Since the size of TMs does not change much within groups, we focus on the first-row TMs to identify interesting electronic configurations. For A-site TMs, the best tolerance factors are always obtained for fluoride compounds. Consequently, we propose $(MA)_3FTi$ as perovskite. The electronic structure (Fig. 3 (a, b)) demonstrates that only TM d bands are in the vicinity of the Fermi level. We observe about four occupied d bands in the α channel (with the highest two being fractionally occupied), whereas 4s bands remain empty at higher energies (not shown). The compound is a half-metal, with empty d states in the β channel. This means, that we do not observe the envisioned filling of e_g states but a high-spin configuration instead. In addition, Ti is approximately neutral. Instead of negative charge on Ti, some MA p orbitals (which are traditionally found at the CBE in IHPs) are filled. Qualitatively this picture is the same at the HSE level. This unfavorable electronic structure leads to a high formation energy of 5.75 eV.

Adding another electron, V^{2-} in $(MA)_3FV$ could in principle adopt a high-spin configuration to a filling of the valence d shell in one spin channel. Although a high-spin configuration with a filled d shell in the α channel is found (Fig. 3 (c,d)), we observe that V also prefers a neutral oxidation state, resulting in another half-metal.

$(MA)_3FMn$ could form a similar half-metal. However, analogous to the Ti compound, we observe a high-spin configuration (not shown). The TM 4s shell remains empty and some of the d_β bands are fractionally occupied, making the assignment of an integer oxidation state ambiguous.

More interesting are the d^8 compounds. Here, the d shell (for divalent anions) is full, and we also observe a full valence 4s shell, i.e., Ni is indeed observed in oxidation state 2-. A gap arises between TM d and p bands (in both groups small band mixing with MA contributions is observed, see Fig. 4 (a,b)). PBE and HSE results for $(MA)_3FNi$ are in very good agreement, other than the band gap increase of about 0.7 eV to 1.11 eV at the HSE level. The influence of SOC (not shown) is small and reduces the band gap by only 0.05 eV at the PBE level. The smallest direct band gap is located at **X** and is only slightly larger (1.15 eV) than the overall band gap. Based on this and the approximation at the HSE level, the true band gap should be well suited for PV applications. To assess the transport properties, we determine the effective masses along the **X**Γ line in the Brillouin zone. While the VB is flat, the CB allows good carrier mobility, with an effective mass of $m^* = 0.88 m_e$ (at the HSE level).

The band gap is tunable by employing heavier d^8 TMs (Pd and

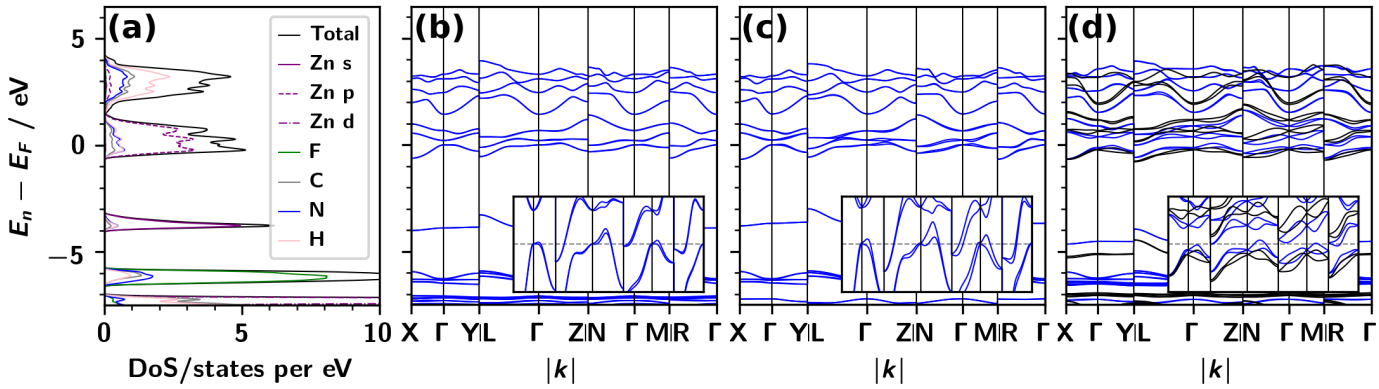

Fig. 1 DoS (a) and band structure (b) of $(MA)_3FZn$, showing filled TM valence s and d shells and TM valence p bands partly filled at the Fermi level. Similar structures with increasing SOC splitting of the p bands are observed for $(MA)_3FCd$ (c) and $(MA)_3FHg$ (d). Insets in the band structure plots show the region around the Fermi level (dashed gray line). In (d), the PBE bands (blue) are compared with HSE (black) results.

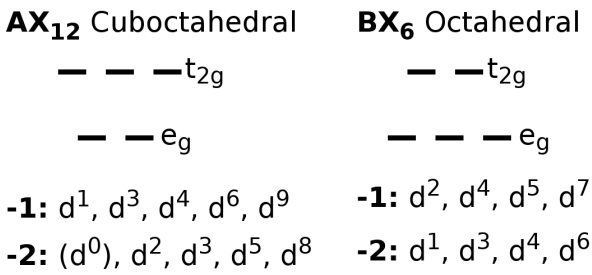

Fig. 2 The d band splitting differs according to the crystal field for TMs on the A- or B-site of perovskites. Consequently, different d-elements yield (half) filled e_g or t_{2g} sets in oxidation states -1 and -2.

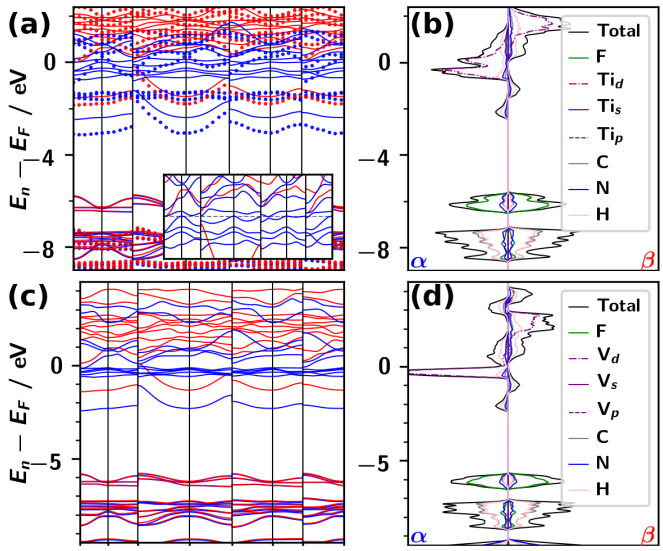

Fig. 3 Spin-polarized band structure and DoS of $(MA)_3FTi$ (a, b) and $(MA)_3FV$ (c, d), respectively. Spin-up (α) and spin-down (β) bands are depicted as blue and red bands in the band structures and plotted to the left and right in the DoS, respectively. Both materials are half-metals, with four and five occupied d_α bands. In (a) we compare PBE bands (solid lines) with HSE bands (dots, only every 20th computed point shown for visibility). The inset in (a) shows the region around the Fermi level (gray line), proving its half metal character.

Pt). Comparing the Pd (Fig. 4 (c)) and Ni compounds, we observe a relative stabilization of the TM d states with respect to the valence s states (see Fig. S1 ESI). As a result, the VBE is located in the Pd $5s$ band at the **L** point. Thus, although a small SOC-induced splitting is observed in the Pd d states, the band gap is not affected by SOC. **L** is also the location of the smallest direct band gap. With 1.59 eV at the HSE level, this gap is perfectly suited for PV applications. The effective masses along **L**Γ for electrons ($0.56m_e$) and holes ($0.49m_e$) indicate excellent charge carrier mobility, in the range of HPs like $MAPbI_3$ and $MASnI_3$.[28]

In contrast, Pt shows a much stronger d band splitting, and, therefore, the VBE is again located at the highest Pt d bands. Consequently, SOC reduces the band gap significantly by 0.3 eV. At the frl-PBE level, the band gap of $(MA)_3FPt$ is with 1.65 eV already at the upper limit for useful PV materials, i.e., the true band gap is likely to be too large for this purpose.

For semiconductor PVs, e.g., the related $MAPbI_3$,[29] it was shown that orbital mixing leading to antibonding states in the valence bands and bonding states in the conduction bands is directly related with defect tolerance.[30] We find such favorable mixing between the TM $d(s)$ and p states and the sp^3 orbitals of MA (see ESI for details), indicating that these materials are likely to host shallow defect levels leading to little carrier recombination.

Thus, $(MA)_3FNi$ and $(MA)_3FPd$ are predicted to be IHPs that are promising PV materials. Note that pinpointing band gaps with electronic structure methods exactly remains challenging and that errors of a few tenth of an electronvolt can be expected with the employed theoretical model. Since TM d bands are usually observed at too high energies, one may speculate that the reported band gaps are slightly underestimated.[31]

The estimated formation energies (0.61 eV to 0.71 eV per formula unit) indicate that these materials could require careful choice of reaction parameters or evolved synthetical concepts.[32] These unfavorable formation energies seems to be a general problem of IHPs containing TMs compared to some main group element compounds. This is in line with the unusual anionic oxidation states for TM, which, however, can be stabilized in alkali, alkaline-earth, or rare-earth metal compounds, as it has been shown, e.g., for group X,[33–38] XI,[37–41] and XII TMs.[37,38]. Stabi-

lization has also been reported with organic ammonium cations such as tetramethylammonium or ammonium.[42–44]

To further tailor the band gap, we modify the halide. First, we increase the size of the halide as *B*-site anion. Since Ni and Pd fluorides already have very promising gaps, we try tuning the Pt compound. In addition, Pt is the largest ion of this group and should accommodate a larger halide best. However, the tolerance factor of $(MA)_3ClPt$ is $t = 0.74$; already below the threshold that allows the perovskite structure. Consequently, we find a considerably distorted structure with PtH bond formation. The band gap of this structure is 3.31 eV at the PBE level, significantly increased compared to the fluoride. Thus, such a modification (Cl for F) is unsuitable for PVs.

Additionally, we examine iodide paired with Pt and Ni. Due to the much increased ionic radius, this change is likely to be accompanied by an interchange of ionic sites and we, therefore, investigate $(MA)_3NiI$ and $(MA)_3PtI$. These compounds with TM metals on the *B*-site show protonation of the TM and further phase changes to allow TM–halide bonds, analogous to findings of light elements in groups XIII and XIV. Thus, this modification is also unsuitable, and the most promising compositions for IHPs in this class are the discussed fluorides.

Other TMs that were identified as possibly useful divalent *B*-site cations show the same proton transfer behavior in the compounds $(MA)_3ScI$ and $(MA)_3CrI$. Thus, we conclude that divalent *B*-site TMs are unlikely to form IHPs.

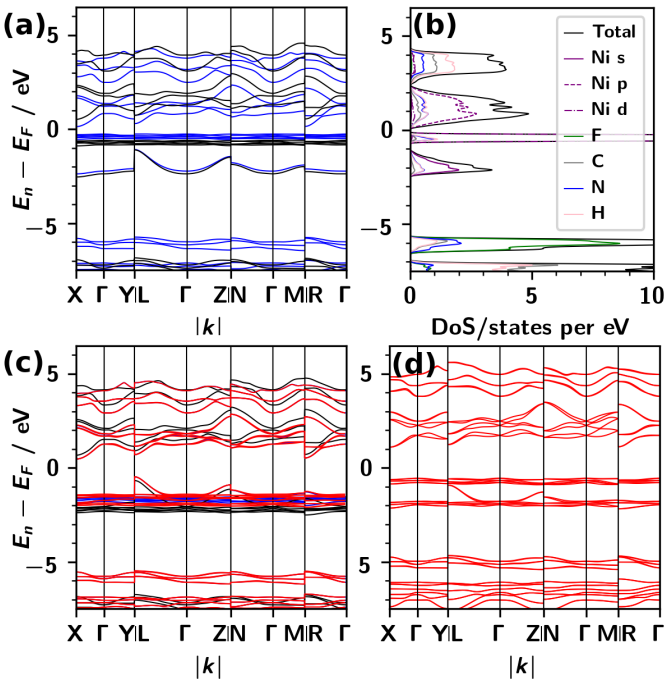

Fig. 4 Band structure (a) and DoS for $(MA)_3FNi$. In (a), bands at PBE (blue) and HSE level (black) are compared, showing an increased gap for HSE but very good agreement otherwise. The DoS reveals that a small gap separates Ni *d* and *p* states. (c) Band structure of $(MA)_3FPb$ comparing srl-PBE (blue), frl-PBE (red), and srl-HSE (black), showing a larger gap, with Pb *s* at the VBE and small splitting of the Pb *d* bands due to SOC. (d) Band structure of $(MA)_3FPt$ at frl-PBE level. The increased *d* band splitting leads to a change at the VBE back to valence *d* states due to the much larger effect of SOC.

3.4 Monovalent anions on the *A*-site

Next, we consider the possibility to form monovalent *A*-site TMs. As mentioned above, the compositional space for these compounds is reduced if we neglect structures with protonated *B*-sites (*B*=O and S).[6] Since all other possible light divalent anions showed the same behavior, currently there does not seem to exist a suitable divalent anion smaller than Se^{2-}. This, however, means that *A*-site anions are required to be very large in order to have good tolerance factors. Consequently, our model compounds $(MA)_3SeAu$, $(MA)_3TeAu$, and $(MA)_3SeV$ all show strong deformations (in addition to protonation in the case of selenides). Solving this issue is likely to require going beyond the realm of inorganic ions, toward more complex design concepts like inverse double hybrid perovskites. This would considerably widen the compositional space but also complicate the materials design. Therefore, such ideas require further studies. For completeness, we demonstrate that the protonation of *B*-site O is also found in TM compounds for the case of $(MA)_3OAu$. The improved tolerance factor compared to the selenide compound leads to a stabilization (E_{form} reduced by 0.89 eV). As expected, water formation is observed at the *B*-site.

3.5 Monovalent anions on the *B*-site

Last, the possibility to employ TMs as monovalent *B*-site anions is investigated. As the largest chalcogenide, we choose Te^{2-} as the partnering *A*-site anion. Most investigated compounds ($(MA)_3TiTe$, $(MA)_3CrTe$, $(MA)_3MnTe$, and $(MA)_3CoTe$) favor distorted structures related to the $A-B$ structure we found for some light *B*-site main-group elements[6], accompanied by *B*-site protonation.

Only d^9 TMs seem to be suitable for the *B*-site. With a filled *d*-shell as a monovalent anion, Cu^- in $(MA)_3CuTe$ is not protonated. As a perovskite, the octahedra open toward one site to allow Cu–Te interactions. However, the tolerance factor is small, $t = 0.79$. Consequently, we find that a distorted $CaIrO_3$ structure similar to $(MA)_3AuTe$ is energetically favorable. The band gap of $(MA)_3CuTe$ is 1.54 eV at the PBE level. With a gap of 2.27 eV for the Au compound, a clear band gap increase with increasing period is observed. Hence, the Ag compound can be expected to have an intermediate band gap of about 1.91 eV. Unfortunately, this means that the realistic band gap of these compounds will be slightly too large for ideal PV applications.

4 Conclusion

Here, we extend our materials search for IHPs to TMs. The site preference for suitable compounds is in line with earlier investigations on main-group metal compounds, although less accurate estimates of anionic radii for TMs in anionic oxidation states lead to a few outliers around the threshold value of $t = 0.76$. In comparison to main group compounds, the different crystal field splitting on *A*- and *B*-sites additionally influences the electronic configuration of TMs. The generally medium to large TM metals are best suited as *A*-site anions in conjunction with fluoride. In this group we observe metallic, half-metallic, and semiconducting IHPs. In particular, d^8 $(MA)_3FA$ compounds are promising.

Table 1 Tolerance factor t, structure information, formation energies E_{form}, and band gap E_g for the investigated MA_3BA compounds. For cases with indirect band gap, the smallest direct band gap E_g^{dir} is given in brackets. Boldface values are results computed at the HSE level. P=perovskite, ?=no tolerance factor could be determined due to a lack of materials of the TM in the envisioned oxidation state, '=structural distortion

System	t	Structure	V/atom/Å^3	a_0/Å	b_0/Å	c_0/Å	α	β	γ	$E_g(E_g^{\text{dir}})/E_g^{\text{frl}}(E_g^{\text{frl,dir}})$/eV	E_{form}/eV
$(MA)_3FZn$	0.88	P	8.28	5.76	6.40	5.87	94.54	92.16	92.35	metallic/metallic,**metallic**	0.60
$(MA)_3FCd$	0.91	P	8.56	5.84	6.43	5.95	94.05	91.85	92.03	metallic/metallic,**metallic**	0.56
$(MA)_3FHg$	0.89	P	8.33	5.75	6.42	5.89	94.20	92.02	92.09	metallic/metallic,**0.19(0.55)**	0.59
$(MA)_3OAu$	0.88	$P(OH_2)$	7.90	5.75	6.33	5.67	94.51	88.99	90.48	2.27 (3.16)	0.51
$(MA)_3SeAu$	0.74	P(SeH)	8.32	6.73	5.72	5.89	81.44	86.17	74.61	2.69 (2.42)	1.40
$(MA)_3CuTe$	0.79	$CaIrO_3$'	8.39	6.33	6.16	5.85	86.76	77.45	78.51	1.54(1.68)	0.47
$(MA)_3AuTe$	0.76	$CaIrO_3$'	8.67	6.33	6.27	5.92	85.47	77.22	79.90	2.27 (2.42)	0.65
$(MA)_3FTi$	0.83	P	8.36	5.94	6.26	5.86	94.43	90.78	89.99	half-metal	5.75
$(MA)_3FV$	?	P	8.02	5.81	6.27	5.73	92.54	90.88	90.25	half-metal	0.84
$(MA)_3FMn$	?	P	8.02	5.79	6.35	5.68	92.83	91.55	90.79	metallic	-1.09
$(MA)_3FNi$	0.79	P	7.33	5.67	6.21	5.41	92.12	90.81	90.39	0.39(0.42)/0.34(0.37),**1.11(1.15)**	0.71
$(MA)_3FPd$	0.85	P	7.48	5.71	6.23	5.47	90.88	90.85	90.02	0.94(1.18)/0.94(1.17),**1.35(1.59)**	0.61
$(MA)_3FPt$	0.84	P	7.32	5.92	6.02	5.41	95.96	83.77	86.48	1.94(2.12)/1.65(1.72)	0.77

With direct band gaps in the range of 1.15 eV to 1.59 eV, low effective masses, and defect tolerance A=Ni and Pd are promising for PV applications. As such, these materials are candidates for the next generation of hybrid perovskite PV crystals.

Acknowledgements

This work was supported by the U.S. Office of Naval Research, under Grant N00014-17-1-2574. J. G. thanks the German Research Foundation for support from Research Fellowships GE 2827/1-1 and GE 2827/2-1. Computational support is provided by the HPCMO of the U.S. DOD.

Notes and references

1 J. Gebhardt and A. M. Rappe, *ACS Energy Lett.*, 2017, **2**, 2681–2685.

2 J. Gebhardt and A. M. Rappe, *Adv. Mater.*, 2018, **Submitted**, year.

3 B. P. Batail, C. Livage, S. S. P. Parkin, C. Coulon, J. D. Martin and E. Canadell, *Angew. Chem. Int. Ed. Engl.*, 1991, **30**, 1498–1500.

4 A. Dhouib, K. Essalah, B. Tangour and M. Abderraba, *Int. J. Quantum Chem.*, 2002, **87**, 220–224.

5 T. Hiramatsu, Y. Yoshida, G. Saito, A. Otsuka, H. Yamochi, Y. Shimizu, Y. Hattori, Y. Nakamura, H. Kishida, H. Ito, K. Kirakci, S. Cordier and C. Perrin, *J. Mater. Chem. C*, 2015, **3**, 11046–11054.

6 J. Gebhardt and A. M. Rappe, *J. Phys. Chem. C*, 2018, 10.1021/acs.jpcc.8b01008.

7 I. E. Castelli, J. M. García-Lastra, K. S. Thygesen and K. W. Jacobsen, *APL Mater.*, 2014, **2**, 081514.

8 M. R. Filip and F. Giustino, *J. Phys. Chem. C*, 2016, **120**, 166–173.

9 T. Nakajima and K. Sawada, *J. Phys. Chem. Lett.*, 2017, **8**, 4826–4831.

10 A. Kojima, K. Teshima, Y. Shirai and T. Miyasaka, *J. Am. Chem. Soc.*, 2009, **131**, 6050–6051.

11 J. H. Noh, S. H. Im, J. H. Heo, T. N. Mandal and S. I. Seok, *Nano Lett.*, 2013, **13**, 1764–1769.

12 M. A. Green, K. Emery, Y. Hishikawa, W. Warta and E. D. Dunlop, *Prog. Photovolt Res. Appl.*, 2015, **23**, 805–812.

13 J. P. Perdew, K. Burke and M. Ernzerhof, *Phys. Rev. Lett.*, 1996, **77**, 3865–3868.

14 P. Giannozzi, S. Baroni, N. Bonini, M. Calandra, R. Car, C. Cavazzoni, D. Ceresoli, G. L. Chiarotti, M. Cococcioni, I. Dabo, A. Dal Corso, S. de Gironcoli, S. Fabris, G. Fratesi, R. Gebauer, U. Gerstmann, C. Gougoussis, A. Kokalj, M. Lazzeri, L. Martin-Samos, N. Marzari, F. Mauri, R. Mazzarello, S. Paolini, A. Pasquarello, L. Paulatto, C. Sbraccia, S. Scandolo, G. Sclauzero, A. P. Seitsonen, A. Smogunov, P. Umari and R. M. Wentzcovitch, *J. Phys. Condens. Matter*, 2009, **21**, 395502.

15 S. Grimme, *J. Comput. Chem.*, 2006, **27**, 1787–1799.

16 A. M. Rappe, K. M. Rabe, E. Kaxiras and J. D. Joannopoulos, *Phys. Rev. B*, 1990, **41**, 1227–1230.

17 N. J. Ramer and A. M. Rappe, *Phys. Rev. B*, 1999, **59**, 12471.

18 I. Grinberg, N. Ramer and A. Rappe, *Phys. Rev. B*, 2000, **62**, 2311–2314.

19 H. J. Monkhorst and J. D. Pack, *Phys. Rev. B*, 1976, **13**, 5188–5192.

20 A. V. Krukau, O. A. Vydrov, A. F. Izmaylov and G. E. Scuseria, *J. Chem. Phys.*, 2006, **125**, 224106.

21 N. Marzari and D. Vanderbilt, *Phys. Rev. B*, 1997, **56**, 12847–12865.

22 Z. Yang, J. Gebhardt, T. A. Schaub, T. Sander, J. Schönamsgruber, H. Soni, A. Görling, M. Kivala and S. Maier, *Nanoscale*, 2018, **10**, 3769–3776.

23 V. M. Goldschmidt, *Naturwissenschaften*, 1926, **14**, 477–485.

24 R. D. Shannon and C. T. Prewitt, *Acta Crystallogr., Sect. B Struct. Crystallogr. Cryst. Chem.*, 1969, **B25**, 925–946.

25 R. D. Shannon, *Acta Crystallogr., Sect. A Cryst. Phys., Diffr., Theor. Gen. Crystallogr.*, 1976, **32**, 751–767.

26 J. Gebhardt and A. M. Rappe, *Comput. Phys. Commun.*, 2018, **Submitted**, year.

27 R. G. Burns, *Mineralogical Applications of Crystal Field Theory*, Cambridge University Press, Cambridge, 2nd edn., 1993.

28 P. Umari, E. Mosconi and F. De Angelis, *Sci. Rep.*, 2014, **4**, 4467.

29 R. E. Brandt, V. Stevanovic, D. S. Ginley and T. Buonassisi, *MRS Commun.*, 2015, **5**, 265–275.

30 A. Zakutayev, C. M. Caskey, A. N. Fioretti, D. S. Ginley, J. Vidal, V. Stevanovic, E. Tea and S. Lany, *J. Phys. Chem. Lett.*, 2014, **5**, 1117–1125.

31 S. Lany, *Phys. Rev. B - Condens. Matter Mater. Phys.*, 2013, **87**, 085112.

32 B. J. Beberwyck, Y. Surendranath and A. P. Alivisatos, *J. Phys. Chem. C*, 2013, **117**, 19759–19770.

33 K. Jonas, *Angew. Chemie Int. Ed. English*, 1975, **14**, 752–753.

34 A. F. Holleman, E. Wiberg and N. Wiberg, *Lehrbuch der Anorganischen Chemie*, de Gruyter, Berlin, 102nd edn., 2007, p. 1725.

35 A. Karpov, J. Nuss, U. Wedig and M. Jansen, *Angew. Chemie*, 2003, **115**, 4966–4969.

36 J. Köhler and J.-H. Chang, *Angew. Chemie*, 2000, **112**, 2077–2079.

37 M.-H. Whangbo, C. Lee and J. Köhler, *Angew. Chemie - Int. Ed.*, 2006, **45**, 7465–7469.

38 J. Köhler and M.-H. Whangbo, *Solid State Sci.*, 2008, **10**, 444–449.

39 V. E. Wood and J. R. Reitz, *J. Phys. Chem. Solids*, 1962, **23**, 229–235.

40 A. Pantelouris, G. Küper, J. Hormes, C. Feldmann and M. Jansen, *J. Am. Chem. Soc.*, 1995, **117**, 11749–11753.

41 I. Doverbratt, S. Ponou, Y. Zhang, S. Lidin and G. J. Miller, *Chem. Mater.*, 2015, **27**, 304–315.

42 W. J. Peer and J. J. Lagowski, *J. Am. Chem. Soc.*, 1978, **100**, 6260–6261.

43 P. D. C. Dietzel and M. Jansen, *Chem. Commun.*, 2001, **0**, 2208–2209.

44 R. P. Sharma, R. Bala, R. Sharma, B. K. Vermani, D. Singh and P. Venugopalan, *J. Coord. Chem.*, 2005, **58**, 309–316.

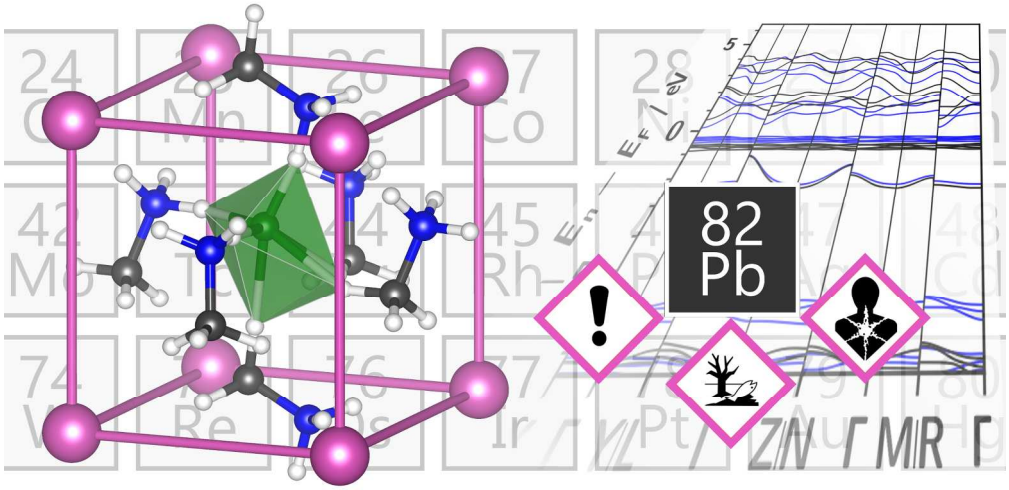
82
Pb
ZN Γ MR Γ